

Discovery of Weak O VI Absorption in Underdense Regions of the Low-Redshift Intergalactic Medium

SAPNA MISHRA ,¹ VIKRAM KHAIRE ,² ROMEO PALLIKKARA ,³ ANAND NARAYANAN ,⁴ AND ANDREW J. FOX ,⁵

¹*Space Telescope Science Institute, 3700 San Martin Drive, Baltimore, MD 21218, USA*

²*Department of Physics, Indian Institute of Technology Tirupati, Tirupati, Andhra Pradesh 517619, India*

³*Department of Physical Sciences, Indian Institute of Science Education and Research (IISER), Mohali, Punjab 140306, India*

⁴*Indian Institute of Space Science & Technology, Thiruvananthapuram, Kerala 695547, India*

⁵*AURA for ESA, Space Telescope Science Institute, 3700 San Martin Drive, Baltimore, MD 21218*

ABSTRACT

We search for weak O VI absorption in the low-redshift intergalactic medium (IGM) using 82 high signal-to-noise quasar spectra obtained with the Cosmic Origins Spectrograph on board the Hubble Space Telescope. From this dataset, we compile a clean sample of 396 intervening Lyman- α (Ly α) absorption lines with H I column densities $\log(N_{\text{HI}}/\text{cm}^{-2}) < 14.5$, all of which lack individual O VI absorption with $\log(N_{\text{O VI}}/\text{cm}^{-2}) > 13$. We perform spectral stacking analysis at the expected location of the O VI doublet, revealing O VI absorption with a statistical significance greater than 5σ , and measure an equivalent width (W_r^{1032}) of $1.7 \pm 0.3 \text{ m}\text{\AA}$, corresponding to $\log(N_{\text{O VI}}/\text{cm}^{-2}) = 12.14 \pm 0.08$. The stacked O VI absorption signal associated with strong Ly α ($13.5 \leq \log N_{\text{HI}} < 14.5$) absorbers is significantly stronger than that associated with the weaker Ly α ($12.5 \leq \log N_{\text{HI}} < 13.5$) absorbers. For the subset of 81 broad Ly α absorbers (BLAs; $b_{\text{HI}} > 45 \text{ km s}^{-1}$), we obtain a marginal $\sim 3\sigma$ O VI detection. Other than Si III, detected at 5σ , no associated metal lines are found. Cross-correlation of the Ly α absorbers with galaxies indicates that 93% of these absorbers are not associated with bright galaxies within 1 Mpc, indicating that the detected O VI originates in the diffuse IGM rather than the circumgalactic medium. The stacked O VI signal suggests characteristic metallicities of $\approx 0.01Z_{\odot}$ under photoionisation and $\approx 0.001Z_{\odot}$ under collisional ionisation conditions, though these estimates are model-dependent and assume that O VI and H I trace the same phase. This study provides the first observational evidence for metal absorption in low-column-density Ly α systems that individually exhibit no detectable metals, placing important constraints on the metal enrichment of the underdense IGM.

Keywords: Intergalactic medium – Intergalactic abundances – Warm-hot intergalactic medium – Voids

1. INTRODUCTION

A comprehensive census of the baryon inventory in the low-redshift universe reveals that observations fall short of expectations, and only account for 30–40% of the baryons predicted by big-bang nucleosynthesis (Fukugita et al. 1998; Lehner et al. 2007; Bregman 2007; Shull et al. 2012; Planck Collaboration et al. 2020). Although fast radio burst observations have recently constrained the total baryon budget (Macquart et al. 2020; Connor et al. 2025), the exact phase in the temperature and density plane of these baryons remains unclear. Simulations of cosmological structure formation (e.g., Davé & Tripp 2001; Martizzi et al. 2019; Tuominen

et al. 2021) suggest that a significant portion of the missing baryons exists in the intergalactic medium (IGM) consisting a diffuse, low-density ($n_{\text{H}} \sim 10^{-6} - 10^{-4} \text{ cm}^{-3}$) warm-hot phase ($T \sim 10^{5-7} \text{ K}$; Cen & Ostriker 1999), referred to as the warm-hot intergalactic medium (WHIM). A large fraction of this WHIM gas cannot be probed with Lyman- α (hereafter, Ly α) absorption lines since the neutral fraction of H I is low ($f_{\text{HI}} \sim 10^{-7}$ to 10^{-5}) and the lines are too broad (with Doppler parameter $b_{\text{HI}} > 45 \text{ km s}^{-1}$) to imprint significant absorption on the spectra (e.g. Narayanan et al. 2010; Tepper-García et al. 2012; Hu et al. 2023). However, there are individual detections of such broad Ly α absorption (BLA) lines, identified via asymmetry in the absorption line profile of nearby strong Ly α absorbers (see e.g. Richter et al. 2006; Savage et al. 2011; Narayanan et al. 2012; Pachat et al. 2016). These individual detections probe only $\sim 10\%$ of the total baryons predicted

in the WHIM (Danforth et al. 2010; Shull et al. 2012; Tejos et al. 2016).

However, there is an alternative approach for investigating the WHIM, involving the detection of highly ionized metal species such as O VI (e.g. Tripp & Savage 2000; Tripp et al. 2008; Savage et al. 2014; Werk et al. 2016), O VII (Nicastro et al. 2018), or Ne VIII (Savage et al. 2005; Narayanan et al. 2009; Meiring et al. 2013; Pachat et al. 2017; Burchett et al. 2018). These ions serve as effective probes of gas with temperatures above 10^5 K when the dominant ionization mechanism is collisional ionization. A significant challenge in these metal absorbers lies in determining the ionization mechanism, as studies have indicated that some of these metals may also arise from low-density photoionized gas (e.g. Hussain et al. 2015, 2017; Chen et al. 2017). Therefore, the interpretation of these observations hinges on the uncertain spectral slopes of extragalactic UV background (see Khaire & Srikanand 2015, 2019; Acharya & Khaire 2022) at the ionization potential of these ions.

Searching for highly ionized gas is important not only for probing the WHIM but also for assessing the metal content within the IGM and the circumgalactic medium (CGM). Previous surveys targeting low-redshift O VI absorption have provided valuable insights (e.g. Tripp et al. 2008; Thom & Chen 2008a,b; Danforth & Shull 2008; Savage et al. 2014; Werk et al. 2016), yielding metallicity measurements of the O VI-bearing gas ranging from $\approx 0.01 - 1 Z_{\odot}$ (Savage et al. 2014; Sameer et al. 2024). These surveys primarily focused on detections of individual O VI absorbers, in most instances with strong associated Ly α absorption with high H I column densities ($\log N_{\text{HI}} > 14.5$). O VI is known to be prevalent in high H I column density clouds due to their vicinity to galaxies and higher oxygen abundances (e.g. Fox et al. 2013; Werk et al. 2016; Sameer et al. 2024), potentially introducing biases into the metallicity estimates for these detections.

Hence, it is important to extend the search for O VI to low-H I column density systems ($\log N_{\text{HI}} < 14.5$), which trace the more diffuse regions of the IGM where the WHIM is predicted to reside. However, detecting individual O VI absorbers in such systems is challenging, as the absorption features will be significantly weak, concealed within the noise of the spectra. The limited signal-to-noise (S/N) of individual sightlines prevents a direct detection of these weak absorbers. To overcome this limitation, we make use of the spectral stacking technique (see e.g., Frank et al. 2018; Lan & Mo 2018; Mishra & Muzahid 2022; Yang et al. 2022; Mishra et al. 2024), which combines the spectral regions corresponding to the expected O VI doublet from a large ensemble of Ly α systems. By co-adding these spectra in the rest frame of the absorbers, random noise averages out; at the same time, any O VI absorption signal is reinforced, thereby enabling the detection of statistically significant but individ-

ually undetectable absorption features. This approach provides a means for measuring the average metal content of the low-density IGM and extending the census of intergalactic metals to regimes inaccessible through individual line detections.

In this study, we explore the high-quality dataset of Danforth et al. (2016, hereafter D16), focusing on the low-redshift IGM. This dataset contains 82 quasar spectra observed with the FUV gratings of the Cosmic Origins Spectrograph (COS) on board the Hubble Space Telescope (HST), with a high S/N of more than 10 per resolution element. We utilize the absorption line identification (IDs) provided by D16 and select a clean, uncontaminated sample of 396 Ly α absorption lines where there is no individual detection of corresponding O VI absorption with $\log N_{\text{OVI}} > 13$. On this sample, we perform the spectral stacking using three different methods: median, S/N weighted mean, and 5σ clipped mean. All three methods yield a clear detection of weak O VI doublet at more than 5σ statistical significance. This represents the first detection of its kind.

This paper is organized as follows: In Section 2, we outline our approach to sample selection. Section 3 describes the stacking analysis methods and Section 4 presents the results obtained from these methods. In Section 5, we discuss the galactic association and metallicity contributed from the detected O VI absorption and its implications on the outcomes. Finally, in Section 6, we provide a concise summary of our findings. Throughout the paper we use a flat Λ CDM cosmology with $H_0 = 70 \text{ km s}^{-1} \text{ Mpc}^{-1}$, $\Omega_M = 0.3$, and $\Omega_{\Lambda} = 0.7$.

2. SAMPLE SELECTION FOR O VI SEARCH

We analyze the D16 low-z IGM dataset containing 82 high S/N (> 10 per resolution element) HST COS quasar spectra observed with G130M and G160M gratings. Most of these quasars are observed under Guaranteed Time Observation programs (PI Green), and some are under Guest Observer programs. The spectra were reduced and co-added by D16. The final spectra with all the line IDs are provided by D16 on the MAST webpage¹.

The D16 quasars probe the Ly α forest at $z < 0.48$. However, our search for O VI and corresponding Ly α lines confines us to a limited redshift range, $0.09 < z < 0.48$. This redshift range ensures the spectral coverage of both O VI doublets and Ly α lines within the COS spectra, spanning wavelengths from 1122 Å to 1800 Å as covered by G130M and G160M gratings. Within this redshift interval, D16 identified a total of 1875 Ly α lines. Among these, 436 exhibited individual O VI detections (with at least one line of the doublet) with $\log N_{\text{OVI}} > 13$ as reported in the same catalog with a

¹<https://archive.stsci.edu/prepds/igm>

tolerance of $\Delta v = 50 \text{ km s}^{-1}$ around the expected O VI locations. We excluded these Ly α lines, resulting in a sample of 1439 Ly α absorption lines without individual O VI detection. Subsequently, for completeness and to avoid inclusion of any misidentified Ly α line, we also removed 132 Ly α lines lying in the geo-coronal Ly α line region ($\sim 1208\text{--}1224 \text{ \AA}$). This resulted in 1307 Ly α absorption lines.

For these 1307 Ly α absorption lines, we searched for contamination from any other lines, including intervening absorption and strong interstellar medium absorption originating from our Milky Way (such as Si II, Si III, Fe II, C II, Si IV, C IV) at the expected locations of O VI $\lambda\lambda 1032, 1038$ doublet lines. For achieving this, we followed the line finding algorithm outlined in D16. To determine individual absorption lines, D16 introduced a significance level (SL) based on equivalent width, defined as $SL(\lambda) = W(\lambda)/\bar{\sigma}(\lambda)$, where W represents the equivalent width of the line and $\bar{\sigma}(\lambda)$ accounts for the error vector convolved with a Gaussian having a Doppler parameter of $b = 20 \text{ km s}^{-1}$ to approximate the COS Line Spread Function (LSF). Spectral regions with $SL \geq 3$ were identified as absorption lines. For each of these systems, we isolated a rest-frame wavelength region spanning from 1030–1040 \AA , encompassing the O VI doublet, and conducted a meticulous search for potential contamination at the expected locations. To find contamination, we utilized the reported b values of the Ly α lines in the D16 catalog and examined if any other absorption lines that were detected within a range of 3 times the Full Width at Half Maximum (FWHM) of the Ly α line ($\text{FWHM} = 2\sqrt{\ln 2} b$). We excluded 721 lines that exhibited contamination from other absorption lines. Excluding these 721 Ly α lines yielded a clean sample of 586 Ly α absorption systems, free of any detected O VI absorption or contamination from other lines at the O VI wavelengths.

Finally, to detect O VI absorption from the diffuse IGM, we considered only systems with Ly α column densities of $\log N_{\text{HI}} < 14.5$. The majority of our Ly α lines at this stage satisfy this criterion, except for seven systems. We therefore excluded these seven from our analysis, resulting in a sample of 579 clean weak Ly α absorption systems. We also required the spectral regions used for detecting the O VI $\lambda\lambda 1032, 1038$ doublet to be free of geocoronal contamination. Therefore, we excluded all Ly α systems for which the expected O VI doublet absorption falls within the geo-coronal emission regions of N I (1198–1202 \AA), Ly α (1208–1224 \AA), or O I (1300–1308 \AA). In addition, we retained only those systems that have at least five uncontaminated pixels within $\pm 51 \text{ km s}^{-1}$ of both O VI doublet lines. This criterion removed an additional 163 Ly α systems, leaving 416 Ly α absorbers. A subsequent visual inspection of these 416 absorbers at the expected O VI doublet locations led to the removal of 20 more systems that showed absorption at the

weaker O VI 1038 line but no corresponding feature at the stronger O VI 1032 line. After implementing these exclusions, the final, clean sample comprises 396 Ly α absorbers.

In Fig. 1, we show the histogram of the column densities of these 396 H I absorbers tracing a subset of low column density Ly α forest region. This carefully curated sample served as the basis for our spectral stacking analysis, aimed at uncovering the presence weak O VI. The specifics of our stacking methods are detailed in the following section.

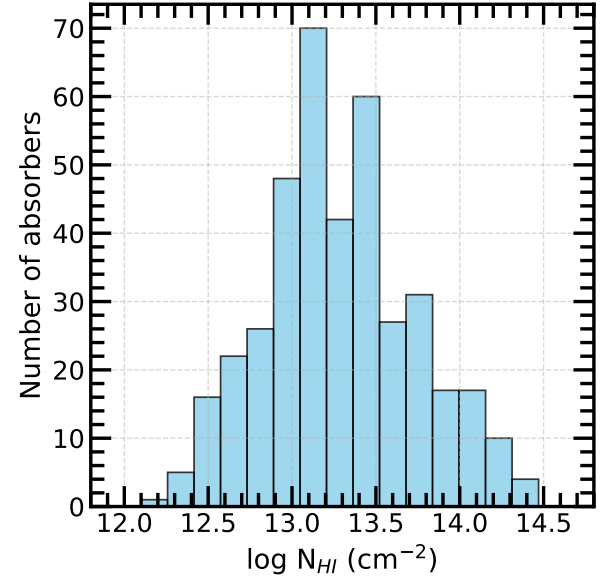


Figure 1. Histogram showing the column density distribution of our final, clean 396 weak H I absorbers that defines our stacking sample to detect weak O VI IGM absorption.

3. SPECTRAL STACKING ANALYSIS

To perform the spectral stack, we first convert the observed wavelength into the rest-frame wavelength by dividing the wavelength array of each Ly α system by $(1 + z_a)$ where z_a is the redshift of the absorber. Subsequently, we segment the wavelength intervals from 1030 to 1040 \AA designated for stacking the O VI doublet. These segments are then rebinned with a consistent pixel separation of 0.03 \AA , as initially defined in D16, corresponding to $\Delta v = 6 \text{ km s}^{-1}$.

In our stacking approach, we do not use the global continuum fits provided by D16. Instead, we opt for a more localized continuum fitting strategy, focusing on the 10 \AA segment of each spectrum to attain more accurate representations of the local continuum variations. For this purpose, we employ an automated code developed by Mishra & Muahid (2022). Briefly, we adopted the continuum from D16 as an initial baseline continuum and normalized the spectrum. We then applied an iterative boxed sigma-clipping procedure with asymmetric sigma levels, chosen based on the median

S/N of each spectrum, to remove absorption features while preserving residual emission. The number of boxes was adjusted depending on the presence of strong emission lines. The iterative clipping was performed until most absorption features were removed. The clipped regions were then linearly interpolated, and a spline was fitted to the residual spectrum, yielding the final continuum.

After fitting the local continuum for all the O VI segments, we proceed to perform spectral stacking using three distinct methods as outlined in detail in [Mishra et al. \(2024\)](#). To summarize, firstly, we implement the median stacking approach, wherein we compute the sample median at each pixel within our rebinned spectra. Our second method employs S/N-weighted mean stacking. Initially, we calculate the S/N for each O VI segment by dividing the normalized flux by the normalized error vector and subsequently taking the median. In this S/N calculation, we exclude the region within $3 \times \text{FWHM}$ of the corresponding Ly α absorption line, as we anticipate the presence of O VI in this region. Following the S/N determination, we assign $1/(\text{S}/\text{N})$ weights to each segment and calculate the weighted mean at each pixel. Our third stacking method involves a 5σ clipped mean. Here, we compute a sample mean at each pixel while clipping any outliers that deviate from the mean by more than 5σ . In this context, σ denotes the standard deviation calculated from normalized flux values at each pixel. The results from these methods are shown in the next section.

4. RESULTS

The stacked profiles from the three different stacking methods are shown in [Fig. 2](#). The vertical dashed lines in each panel denote the expected positions of the O VI doublet. In all three cases, the spectral stacks exhibit clear absorption coinciding with the anticipated location of both lines of the O VI doublet. The expected O VI absorption is superimposed on a broad, emission-like feature as can be seen in [Fig. 2](#) left panel. This broad emission-like feature arises because we ensured that the $\pm 50 \text{ km s}^{-1}$ shaded region around the O VI doublet is free from any contaminating absorption. However, spectral regions beyond this window may contain unrelated random absorption, which can cause the stacked profiles to appear slightly suppressed in these regions (as also shown in [Mishra et al. 2024](#)).

To mitigate these effects, we fitted a pseudo-continuum to these stacks. We employed the similar continuum fitting approach of iterative sigma-clipping and spline-fitting procedure used for the individual spectrum. The fit excluded the $\pm 50 \text{ km s}^{-1}$ region corresponding to the O VI doublet. The distinctive bump observed at the O VI doublet location warranted the use of higher spline knots (~ 10) during the continuum fitting process. The resulting pseudo-continuum is shown by solid green lines in the left-hand panel of [Fig. 2](#).

Subsequently, we utilized this continuum for further normalizing the spectral stack, the results of which are displayed in the right-hand panel of [Fig. 2](#). Within the normalized stack, the absorption features of both O VI doublet lines are prominently visible at their anticipated positions.

To calculate the significance of detection in the final stack, we rebin the stack to have the pixel size of the COS resolution element (i.e with $\delta v = 18 \text{ km s}^{-1}$) by smoothing and rebinning it by 3 pixels. Then the significance of detection of each line in the final stacks, we determined the significance level SL of the absorption line by calculating $SL^2 = \sum_i [(1 - f_i)/\sigma]^2$ where f_i is the flux at i^{th} pixel within $\pm 50 \text{ km/s}$ of the absorption line and σ is standard deviation of flux excluding the region where we expect the O VI. For the spectral stack including both lines of the doublet, we determine a combined significance of $SL = \sqrt{S_{1032}^2 + S_{1038}^2}$, which is 5.6σ (5.0σ for the blue and 2.5σ for the red component) for our median stack, 6.2σ (5.4σ for the blue and 3.1σ for the red component) for our S/N-weighted mean stack, and 5.7σ (4.7σ for the blue component and 3.2σ for the red component) for our 5σ clipped mean stack. In all three cases, the blue line is detected at $\approx 5\sigma$, while the red line is detected at $2.5\text{--}3.2\sigma$. Consequently, the combined detection significance of the doublet across the stacks is $\approx 6\sigma$. The measured rest-frame equivalent widths for the O VI 1032 \AA (W_r^{1032}) are determined to be $2.0 \pm 0.3 \text{ m\AA}$ (median stack), $1.7 \pm 0.3 \text{ m\AA}$ (S/N-weighted mean stack), and $1.8 \pm 0.4 \text{ m\AA}$ (5σ -clipped mean stack). The doublet ratios (DR) measured for the detected O VI absorption are 1.9 ± 1.2 , 1.4 ± 0.8 , and 1.3 ± 0.7 for the median, S/N-weighted mean, and 5σ -clipped mean stacks, respectively. Within the quoted uncertainties, these values are consistent with the expected optically thin ratio of $DR = 2$. However, the relative strengths of the two components are sensitive to the placement of the local continuum due to the weak nature of the signal. Besides the global pseudo continuum shown here, we tested alternative continuum fits (spline + polynomial, splines with varying knots across the spectral region). We confirm different methods yield DR and EW values consistent within their quoted uncertainties.

Although our stacking methods provide means to recover weak absorption features, the approach carries potential caveats. The stacking procedure assumes that the “hidden” O VI features are perfectly aligned with the corresponding H I Ly α redshifts. Any systematic offset between the O VI and H I centroids (on the order of tens of km s^{-1}) will broaden and weaken the stacked signal, potentially leading to an underestimation of the stacked O VI equivalent width. For higher-column-density Ly α absorbers, the O VI and the strongest H I components are misaligned in as many as 60% of cases (see [Tripp et al. 2008](#)). Indeed, such misalignments are expected in a multiphase medium. The “non-aligned”

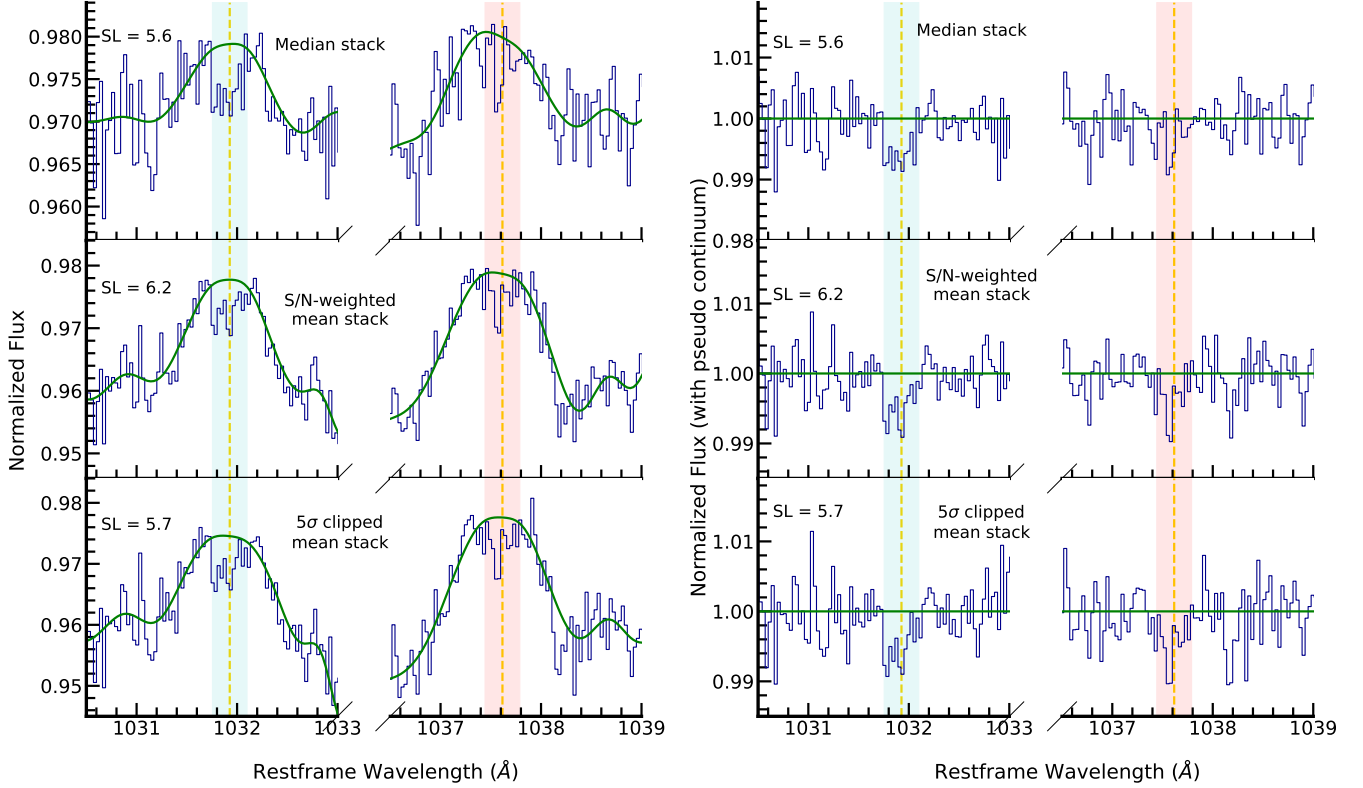


Figure 2. Stacked O VI absorption profiles obtained through three methods: median (top panels), S/N-weighted mean (middle panels), and 5σ clipped mean. Vertical dashed lines represent the expected O VI doublet locations, while the shaded regions encompass the $\pm 50 \text{ km s}^{-1}$ around absorption features. The left-hand panels depict the stacked profiles with pseudo-continuum (green curve), while the right-hand panels show the pseudo-continuum normalized stacks. All three methods yield O VI absorption with a statistical significance of $> 5\sigma$ (legends indicate the combined significance of detection for both lines in each method, see Section 4).

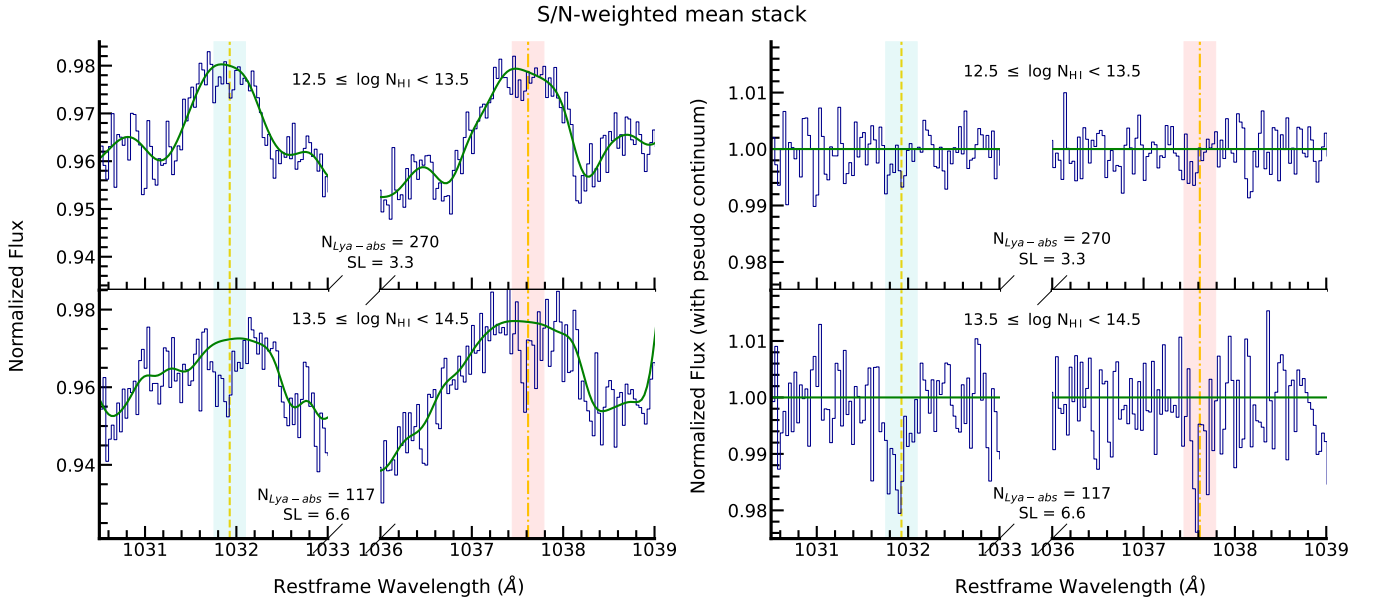


Figure 3. Similar to Fig. 2, this figure displays stacked O VI absorption profiles obtained using the S/N-weighted mean method, with results presented separately for two bins of H I column density: $12.5 < \log N_{\text{HI}} < 13.5$ (top panels, 3.3σ detection) and $13.5 < \log N_{\text{HI}} < 14.5$ (bottom panels, 6.6σ detection).

O VI typically occurs in systems where the O VI is tracing

warm-hot gas with sufficiently high metallicity that the as-

sociated broad H I absorption becomes too weak to detect (Savage et al. 2010). There are also instances of low column density Ly α absorbers ($\log N_{\text{HI}} \geq 13.1$) where the associated O VI is offset in velocity from the Ly α (Williger et al. 2006). Therefore, this possibility cannot be completely ruled out even for weak O VI absorbers.

As also demonstrated in Mishra et al. (2024, see their Appendix B), median stacking method may yield biased results when the S/N distribution within the data is not uniform. Conversely, σ -clipped stacking can lead to the removal of a substantial number of data points, introducing more noise into the stack. Given these considerations and the fact that our sample exhibits a skewed S/N distribution around the median S/N of ~ 15 , we opt to employ the S/N-weighted mean stacking method for our subsequent analysis and present the resulting measurements in Table 1.

In addition to EW, we also provide the column density of stacked O VI using the linear part of the curve-of-growth (COG) using the standard equation (e.g. Petitjean 1998):

$$N^{1032} = 1.13 \times 10^{20} \frac{W_r^{1032}}{f_{1032} \lambda_{1032}^2} \text{ cm}^{-2} \quad (1)$$

Where W_r^{1032} , f_{1032} and λ_{1032} are the rest frame EW, oscillator strength, rest wavelength of the O VI 1032 line. Given the small values of EW (see Table 1, Column 6), the use of a linear COG is justified. Additionally, in the Table 1 we provide the median z , mean N_{HI} and mean b_{HI} values from the sample using the reported values in D16 catalogs.

4.1. Spectral Stacking for Ly α Subsamples

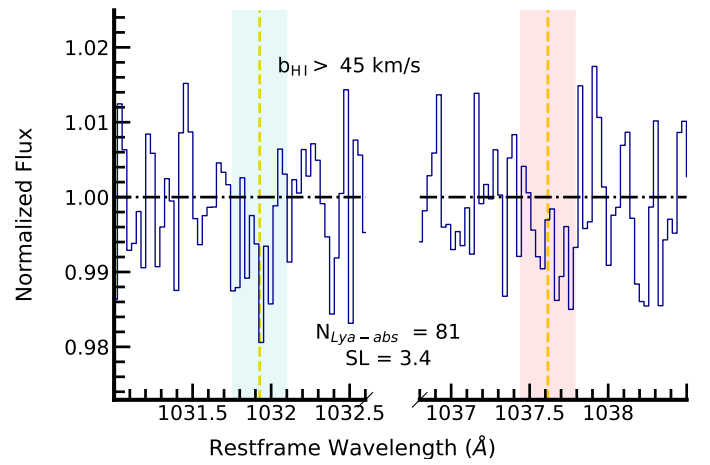
To further investigate the origin of our detected O VI absorption, we divided our sample into two distinct bins based on N_{HI} values: a high-column density sample having $13.5 < \log N_{\text{HI}} < 14.5$, comprising 117 systems, and a low-column density sample having $12.5 < \log N_{\text{HI}} < 13.5$, comprising 270 systems. We removed 9 systems with $\log N_{\text{HI}} < 12.5$ when creating these bins. For both of these bins, we performed stacking on the O VI segments using our S/N-weighted mean stacking method and subsequently conducted pseudo-continuum fits, following the procedure outlined earlier. The resultant stacks, both with and without pseudo-continuum normalization, are presented in Fig. 3. In the high-column density bin, we find a more pronounced O VI doublet as compared to the low-column density bin, featuring W_r^{1032} of $3.6 \pm 0.7 \text{ m}\text{\AA}$ at statistical significance of 6.6σ (5.7σ for the blue and 3.4σ for the red) with DR of 1.3 ± 0.7 . The low-column density bin exhibits W_r^{1032} of $1.1 \pm 0.4 \text{ m}\text{\AA}$ at statistical significance of 3.3σ (3.1σ for the blue and 2.2σ for the red) and DR of 1.2 ± 0.9 .

Further, to investigate whether the gas is associated with the WHIM, we created a BLA sub-sample comprising Ly α lines with broad profiles, characterized by $b > 45 \text{ km s}^{-1}$

(Richter et al. 2006; Danforth et al. 2010). Out of the initial 396 systems, 81 systems met this criterion. We subsequently conducted spectral stacking on these 81 systems in an attempt to detect O VI. As depicted in Fig. 4.1, we detect a marginal detection of O VI in this sub-sample at W_r^{1032} of $2.2 \pm 0.7 \text{ m}\text{\AA}$ significant level of 3.4σ (2.2σ for the blue and 2.6σ for the red). A larger sample of BLAs is required to confirm the statistical significance of the detected O VI absorption.

To explore associated metals alongside our detected O VI, we focused on the Si II $\lambda 1193$ and Si III $\lambda 1206$ lines. We selected these ions due to their proximity in wavelength to the Ly α lines, thereby ensuring comprehensive coverage of the anticipated spectral region within our sample. Following the same contamination removal procedure employed for the O VI segments, we removed any contamination at the locations corresponding to these ions. Subsequently, out of the initial 396 systems, we retained 263 systems for Si II and 259 systems for Si III. Employing the S/N-weighted mean stacking method for both ions, we obtained detection of Si III with a significance of 5.1σ , while no detection for Si II. These results provide equivalent width of $2.5 \pm 0.5 \text{ m}\text{\AA}$ for Si III and an upper limit (3σ) of $< 0.5 \text{ m}\text{\AA}$ for Si II.

We verified that if we stack Ly α absorption lines in our sample with S/N weighted mean and obtain N_{HI} by fitting the Voigt profile to the stack, the fitted N_{HI} and b_{HI} values match closely (within 0.05 dex) with the sample mean (Column 4 and 5 of Table 1). Therefore, for the subsequent analysis, we adopt the mean N_{HI} and b_{HI} values from Table 1 to estimate the metallicities of O VI absorption in the different subsets.



5. DISCUSSION

We detect weak O VI absorption from the low- z IGM at $> 5\sigma$ significance by stacking 396 weak ($\log N_{\text{HI}} < 14.5$) Ly α absorbers from the D16 sample. To compare the column density of our stacked O VI detection with the column

Table 1. Summary of Measurements Performed on S/N-weighted Mean Stacks

Sample	$N_{\text{Ly}\alpha}$	z_{sys}	$\langle \log N_{\text{HI}} \rangle$	$\langle b_{\text{HI}} \rangle$	W_r^{1032}	SL_{1032}	W_r^{1038}	SL_{1038}	$\log N_{\text{OVI}}$
(1)	(2)	(3)	(4)	(5)	(6)	(7)	(8)	(9)	(10)
Full	396	0.19	13.2 ± 0.4	31.25	0.0017 ± 0.0003	5.4	0.0013 ± 0.0003	3.1	12.14 ± 0.08
$12.5 \leq \log N < 13.5$	270	0.19	13.1 ± 0.3	29.55	0.0011 ± 0.0004	3.1	0.0011 ± 0.0004	2.2	11.95 ± 0.15
$13.5 \leq \log N < 14.5$	117	0.24	13.8 ± 0.3	36.9	0.0036 ± 0.0007	5.7	0.0027 ± 0.0007	3.4	12.45 ± 0.08
BLA ($b > 45 \text{ km s}^{-1}$)	81	0.21	13.4 ± 0.4	55	0.0022 ± 0.0008	2.2	0.0021 ± 0.0008	2.6	12.25 ± 0.16

Notes – (1) Sample name.
 (2) Number of $\text{Ly}\alpha$ systems.
 (3), (4), (5) Median redshift, H I column density, and $\text{Ly}\alpha$ b -value.
 (6) REW of O VI 1032 measured within $\pm 50 \text{ km s}^{-1}$ from the S/N-weighted mean stacked spectra; the 1σ uncertainties are derived from 200 bootstrap realizations.
 (7) Detection significance of the O VI 1032 line.
 (8) Same as (6), but for the O VI 1038 line.
 (9) Same as (7), but for the O VI 1038 line.
 (10) O VI column density estimated from the 1032 line using the linear part of the curve of growth.

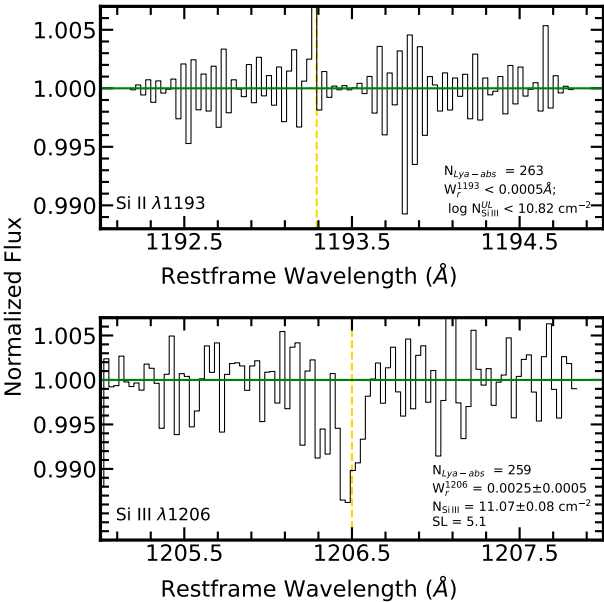


Figure 4. Pseudo-continuum normalized S/N-weighted mean stacks for Si II $\lambda 1193$ (top) and Si III $\lambda 1206$ (bottom). The number of $\text{Ly}\alpha$ absorbers, the upper limit in the Rest-frame Equivalent Width (REW) and column density is given in the bottom right side of each panel.

densities of individually detected O VI absorbers in the low- z IGM, we again used the D16 catalog, which constitutes the largest low- z IGM metal line survey currently available. We selected all individual O VI 1032 systems from their sample of 82 AGN sightlines that show O VI detections within $\pm 3 \times \text{FWHM}$ of the b -value of the associated H I absorbers, and we retained only those with reliable fitting flags both on $\text{Ly}\alpha$ and O VI lines. This selection yielded 247 individual O VI absorbers. Additionally, we excluded six absorbers with column density uncertainties more than 2 dex, result-

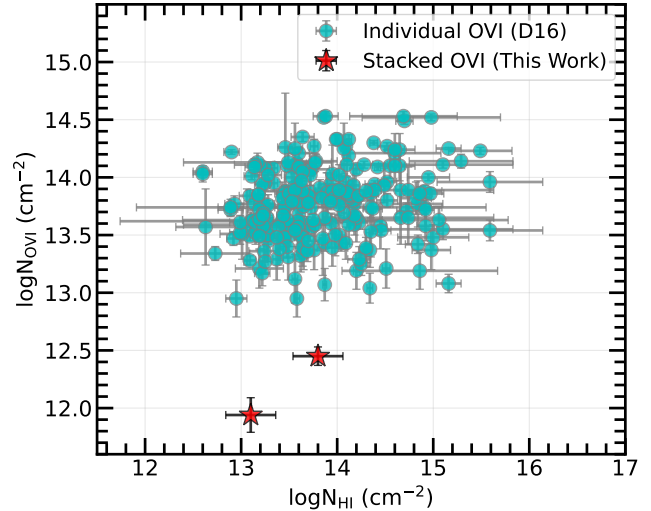


Figure 5. Column densities of H I and O VI for individual absorbers from D16 are shown in cyan circles. The weak O VI absorbers obtained from our stacking analysis for the two bins of $\log N_{\text{HI}}$ are shown as red stars.

ing in a final sample of 241 individual O VI absorbers from D16.

The column densities of these 241 individual D16 O VI absorbers are shown as a function of the corresponding H I column densities in Fig. 5 as cyan circles. The column densities derived from our stacked O VI detections for the two $\log N_{\text{HI}}$ bins (see Table 1) are shown as red stars at the mean H I column density of each bin. Our stacked O VI measurements occupy the lowest region of the N_{OVI} parameter space ever probed in the IGM. Whereas CGM O VI measurements tend to cluster around $\log N_{\text{OVI}} \approx 14.5$ (Heckman et al. 2002; Fox 2011; Tumlinson et al. 2013; Werk et al. 2016), and the D16

catalog of individual IGM O VI absorbers covers the region $13 < \log N_{\text{O VI}} < 14.5$, our stacked O VI signal traces an *entirely new parameter space*, >100 times weaker than the typical CGM O VI signal. The lowest previously reported O VI column density is $\log N_{\text{O VI}} \approx 12.38$, observed only in the local ISM (Savage & Lehner 2006). In the following subsections, we investigate the galaxy associations and metallicity of our detected O VI absorption.

5.1. Association with Galaxies

The O VI ion is frequently detected in the CGM of galaxies, typically within distances of up to $1 - 2$ virial radii (see Tumlinson et al. 2017, for a review). Given the focus of our study on low-column density Ly α absorbers in the search for O VI, we explored whether these systems are situated in proximity to known galaxies. To investigate this, we conducted a search in the Sloan Digital Sky Survey (SDSS-IV) archive (Ahumada et al. 2020) using *CasJobs*². Of the full sample of 396 Ly α absorbers toward 57 quasars, 311 absorbers along 44 quasar sightlines fall within the SDSS sky-coverage footprint.

Around these 311 Ly α absorbers, following the approach of Narayanan et al. (2018), we searched for galaxies with spectroscopic redshifts consistent with each Ly α absorber within a velocity window of $\pm 1000 \text{ km s}^{-1}$ and a projected search radius of 1 Mpc. Within this parameter space, 290 Ly α absorbers toward 43 quasars show no galaxies within $\pm 1000 \text{ km s}^{-1}$ down to $r\text{-mag} < 19.7$, while only 21 absorbers have associated galaxies, with 30 spectroscopic galaxies with a median magnitude of $r\text{-mag} = 18$. When the projected search radius is increased to 5 Mpc, 212 Ly α absorbers toward 41 quasars show no associated spectroscopic galaxies. Galaxies were identified around the remaining 99 Ly α absorbers toward 28 quasars, yielding a total of 279 galaxies in this case. We do not attempt to include galaxies with photometric redshifts in this analysis. Even the most reliable SDSS photometric redshifts (with “photoErrorClass” values of -1 , 1 , 2 , or 3) have typical uncertainties of $\Delta z \approx 0.03$ (Beck et al. 2016). At the median redshift of our sample ($z \sim 0.2$), this corresponds to a velocity uncertainty of $\sim 7000 \text{ km s}^{-1}$ equivalent to a projected separation of ~ 100 Mpc, which is far too large to yield any meaningful constraints on CGM association. Consequently, $\sim 93\%$ ($\sim 68\%$) of the Ly α absorbers in our sample have no galaxies within 1 Mpc (5 Mpc). Hence the detected O VI possibly originates from the IGM. However, future deep surveys are needed to further confirm whether the detected O VI is not associated with the CGM of faint dwarf galaxies, below the detection limits of current surveys.

2

<https://skyserver.sdss.org/casjobs/>

5.2. Metallicity

In order to measure the metallicity of detected O VI, we need to understand the ionization mechanism. If the origin of O VI is predominantly photoionization, then the ionization correction depends on the gas density. However, to obtain density it is usually preferred to have measured column densities of the ions of the same elements. This is the reason why we searched for Si II and Si III. However, because we do not have clear detection of the Si II, we resort to inferring the gas density from hydrodynamic simulations of the IGM.

Simulations of the IGM at low redshift have revealed a robust power-law relation between the overdensity parameter Δ and the Ly α column density, expressed as $\Delta = \Delta_0 N_{14}^\gamma$ (e.g., Davé et al. 2010; Smith et al. 2011; Tepper-García et al. 2012; Gaikwad et al. 2017). In this equation, Δ represents the overdensity, defined as the ratio of the hydrogen number density (n_H) to the mean hydrogen density of the IGM (\bar{n}_H) at redshift z . The parameters Δ_0 and γ denote the normalization and power-law index, respectively. For our analysis, we adopt the values $\Delta_0 = 34.8$ and $\gamma = 0.77$ from Gaikwad et al. (2017), which are consistent with previous estimates (Davé et al. 2010; Smith et al. 2011). These values correspond to $\Delta = 8$ for our entire sample and $\Delta = 7$ and $\Delta = 24$ for the binned samples of low and high N_{HI} , respectively. Using our adopted cosmology parameters, we determine the mean hydrogen density $\bar{n}_H(z) = 1.87 \times 10^{-7} \text{ cm}^{-3}(1+z)^3$, resulting in $\log n_H = -5.6$ for the full sample and $\log n_H = -5.7$ and -5.0 for the binned samples of low and high N_{HI} , respectively.

With these density values in hand, we perform photoionization equilibrium calculations using the CLOUDY code (Gunnasekera et al. 2025). In our models, we incorporate the extragalactic UV background model developed by Khaire & Srianand (2019) for the ionizing background (their fiducial Q18 model) and apply stopping criteria based on the median H I column density of the sample, as outlined in Table 1. Our analysis yields a metallicity of $\log (Z/Z_\odot) = -1.9$ for the full sample (i.e. $0.012 Z_\odot$). Similarly, for the column density binned sample, we obtain comparable results, with $\log (Z/Z_\odot) = -1.8$ (i.e. $0.016 Z_\odot$) for the low N_{HI} bin and -2.2 (i.e. $0.006 Z_\odot$) for the high N_{HI} bin.

On the other hand, if the O VI originates in gas in collisional ionization equilibrium (CIE) at $T = 10^{5.5} \text{ K}$, where the fraction of O VI gas is at its highest (Sutherland & Dopita 1993; Gnat & Sternberg 2007), the metallicity of gas is given by the expression $\log (Z/Z_\odot) = \log N_{\text{O VI}} - \log N_{\text{HI}} - 5.22 + 3.31$, where the number -3.31 is the abundance (O/H) of Sun (Grevesse et al. 2010), and 5.22 is the log of the ratio of ionization fraction of O VI and H I in a CIE model at $10^{5.5} \text{ K}$. Using this expression, we find that, if O VI traces same H I column density as the median of Ly α sample, then the metallicity of O VI bearing gas is $\approx 0.001 Z_\odot$. This inferred metallicity is highly temperature-sensitive and can vary from ≈ 2

to $10^{-4} Z_{\odot}$ for $T = 10^{5-6}$ K. We adopt $T = 10^{5.5}$ K because this temperature corresponds to the peak O VI ion fraction in CIE of 0.22 (Gnat & Sternberg 2007). The resulting metallicity should therefore be regarded as a lower limit, since not all of the observed O VI necessarily arises from collisionally ionized gas. Additional uncertainties can arise because the measured column of H I may not trace gas with the same temperature, kinematics, or line width as the O VI-bearing phase, and the adopted gas temperature may not be consistent with CIE conditions.

The metallicity associated with the lowest column density Ly α absorbers ($\log N_{\text{HI}} < 14$) at $z < 0.5$ is key probe of the chemical enrichment of the diffuse IGM, but remains poorly constrained due to observational limitations. These absorbers arise in low-density regions of the cosmic web ($\Delta \approx 10$), where metal lines are intrinsically faint and fall below the detection thresholds of individual UV spectra. D16 survey showed that the fraction of metal-bearing absorbers drops steeply with decreasing N_{HI} : for $\log N_{\text{HI}} < 13.5$, only $\sim 3\%$ of systems show detectable metals, rising to $\sim 22\%$ for $13.5 < \log N_{\text{HI}} < 14.5$, and becoming nearly ubiquitous only for $\log N_{\text{HI}} > 14.5$. This trend is attributed both to instrumental sensitivity limits and to genuinely lower metallicities in the most diffuse IGM. Cosmological simulations predict that the under-dense $z \approx 0$ IGM should contain only trace metals in the range of $\approx 10^{-3} - 10^{-2} Z_{\odot}$, with the scatter in the estimate due to differences in the feedback model and local enrichment history (Aguirre et al. 2001; Shen et al. 2010; Cen & Chisari 2011). As pointed out earlier, low-redshift O VI surveys have been sensitive only to $\log N_{\text{O VI}} \geq 13$ (Tripp et al. 2008; Danforth & Shull 2008; Savage et al. 2014), corresponding to much stronger Ly α systems potentially associated with the CGM gas. Stacking has probed the average metal absorption, associated with lower N_{HI} systems, that are individually undetectable. Our measurements provide, for the first time, observational evidence of metals even in the weakest Ly α absorbers at $z < 0.5$, placing important constraints on the metal-enriched fraction of the diffuse IGM.

The spectral stacking method demonstrated here offers a pathway to probing any potential metallicity floor in the low-redshift IGM. Identifying such a floor would provide valuable insight into when and how the IGM was enriched by galactic outflows, and would place important constraints on feedback processes in galaxy formation (see e.g., Simcoe et al. 2004; Schaye et al. 2007). Our photoionization modeling resulted in a lowest metallicity estimate of $0.006 Z_{\odot}$ when we stacked O VI in our subsample of H I with $13.5 < \log N_{\text{HI}} < 14.5$ whereas we find $0.016 Z_{\odot}$ for subsample of H I with $12.5 < \log N_{\text{HI}} < 13.5$. Simulations also show that lower column density systems can have metallicities well below $0.01 Z_{\odot}$, consistent with accretion of metal poor IGM gas onto galaxies (Hafen et al. 2017; Rahmati & Oppenheimer

2018). There is no evidence for a universal metallicity floor at or above $0.01 Z_{\odot}$ but this value is consistent with the mean metallicity inferred for the low- z IGM (see Prochaska et al. 2017; Oppenheimer et al. 2012; Shull et al. 2014). Taken together, our results highlight that while the mean metallicity of the low-redshift IGM is of order $0.01 Z_{\odot}$ obtained with the assumptions of photoionization origin of detected O VI gas, the absence of a detectable lower bound in our stacked measurements underscores that the true metallicity floor, if it exists, must lie below this level.

6. CONCLUSIONS

In our study, we employed a spectral stacking method to unveil the presence of O VI absorption lines within the low-column density Ly α absorbers. Our dataset consisted of 82 high S/N quasar spectra from HST-COS, probing the IGM at $z < 0.5$. Our initial screening aimed to identify Ly α absorbers that lacked any individual detections of O VI ($\log N_{\text{O VI}} \gtrsim 13$). We successfully identified 396 such absorbers at $0.1 < z < 0.5$ and confirmed that they were uncontaminated at the expected O VI locations.

Using this set of 396 absorbers, we carried out spectral stacking through three distinct methods, leading to the detection of O VI doublets (Fig. 2). These detections show equivalent width W_r^{1032} of $1.7 \pm 0.3 \text{ m}\text{\AA}$ at significance level of 6.2σ with a corresponding O VI column density of $\log N_{\text{O VI}} = 12.14 \pm 0.08$ in the S/N-weighted mean stack spectrum, around ≈ 1 dex weaker than any individual detectable O VI component.

Upon dividing our absorber sample into two bins based on H I column density, low-column density ($12.5 \leq \log N_{\text{HI}} < 13.5$) and high-column density ($13.5 \leq \log N_{\text{HI}} < 14.5$), we found that the O VI absorption EW in the high-column-density bin is stronger than in the low-column-density bin by more than 3σ .

Out of these 396 systems, we created a sample of potential broad Ly α alpha absorbers containing 81 Ly α lines having $b_{\text{HI}} > 45 \text{ km s}^{-1}$ and performed spectral stack to detect O VI. Our search yields a marginal detection (Fig. 4.1) of O VI with W_r^{1032} of $2.2 \pm 0.7 \text{ m}\text{\AA}$ at 3.4σ and column density of $\log N_{\text{O VI}} = 12.25 \pm 0.16$. A larger BLA sample is needed to confirm this result. Our results are summarized in Table 1.

We further investigated the presence of other metal absorbers associated to O VI focusing on stacking Si II and Si III lines. Our findings included no detection of Si II, and a 5σ detection for Si III, revealing an equivalent width of $2.5 \pm 0.5 \text{ \AA}$ and a corresponding column density of $\log N_{\text{Si III}} = 11.07 \pm 0.08$ (Fig. 4).

We confirm that 93% of our Ly α absorbers do not trace any galaxies within 1 Mpc distance. Hence the O VI absorption reported here is likely originating from the low density IGM. Future deep surveys will be essential to further confirm

whether the detected O VI is not associated with the CGM of faint dwarf galaxies. The overdensities inferred for these weak O VI systems ($\Delta \approx 7 - 24$) place them in the diffuse to mildly overdense regions of large-scale filaments.

In terms of gas metallicity, the detected O VI traces gas with an average metallicity of $\approx 0.01 Z_{\odot}$ in the case of photoionization, and $\approx 0.001 Z_{\odot}$ in the case of collisional ionization at $10^{5.5}$ K in the WHIM. This study probes the average metal absorption associated with low-column density Ly α systems that are individually undetectable, providing the

first observational evidence of metals in the weakest Ly α absorbers at $z < 0.5$ and placing important constraints on the metal-enrichment of the underdense IGM and a possible metallicity floor.

Acknowledgments:

This research is based on observations made with the NASA/ESA Hubble Space Telescope obtained from the Space Telescope Science Institute, which is operated by the Association of Universities for Research in Astronomy, Inc., under NASA contract NAS 5-26555.

REFERENCES

Acharya, A., & Khaire, V. 2022, MNRAS, 509, 5559, doi: [10.1093/mnras/stab3316](https://doi.org/10.1093/mnras/stab3316)

Aguirre, A., Hernquist, L., Schaye, J., et al. 2001, ApJ, 561, 521, doi: [10.1086/323370](https://doi.org/10.1086/323370)

Ahumada, R., Allende Prieto, C., Almeida, A., et al. 2020, ApJS, 249, 3, doi: [10.3847/1538-4365/ab929e](https://doi.org/10.3847/1538-4365/ab929e)

Beck, R., Dobos, L., Budavári, T., Szalay, A. S., & Csabai, I. 2016, MNRAS, 460, 1371, doi: [10.1093/mnras/stw1009](https://doi.org/10.1093/mnras/stw1009)

Bregman, J. N. 2007, ARA&A, 45, 221, doi: [10.1146/annurev.astro.45.051806.110619](https://doi.org/10.1146/annurev.astro.45.051806.110619)

Burchett, J. N., Tripp, T. M., Prochaska, J. X., et al. 2018, arXiv e-prints. <https://arxiv.org/abs/1810.06560>

Cen, R., & Chisari, N. E. 2011, ApJ, 731, 11, doi: [10.1088/0004-637X/731/1/11](https://doi.org/10.1088/0004-637X/731/1/11)

Cen, R., & Ostriker, J. P. 1999, ApJ, 514, 1, doi: [10.1086/306949](https://doi.org/10.1086/306949)

Chen, H.-W., Johnson, S. D., Zahedy, F. S., Rauch, M., & Mulchaey, J. S. 2017, ApJL, 842, L19, doi: [10.3847/2041-8213/aa762d](https://doi.org/10.3847/2041-8213/aa762d)

Connor, L., Ravi, V., Sharma, K., et al. 2025, Nature Astronomy, 9, 1226, doi: [10.1038/s41550-025-02566-y](https://doi.org/10.1038/s41550-025-02566-y)

Danforth, C. W., & Shull, J. M. 2008, ApJ, 679, 194, doi: [10.1086/587127](https://doi.org/10.1086/587127)

Danforth, C. W., Stocke, J. T., & Shull, J. M. 2010, ApJ, 710, 613, doi: [10.1088/0004-637X/710/1/613](https://doi.org/10.1088/0004-637X/710/1/613)

Danforth, C. W., Keeney, B. A., Tilton, E. M., et al. 2016, ApJ, 817, 111, doi: [10.3847/0004-637X/817/2/111](https://doi.org/10.3847/0004-637X/817/2/111)

Davé, R., Oppenheimer, B. D., Katz, N., Kollmeier, J. A., & Weinberg, D. H. 2010, MNRAS, 408, 2051, doi: [10.1111/j.1365-2966.2010.17279.x](https://doi.org/10.1111/j.1365-2966.2010.17279.x)

Davé, R., & Tripp, T. M. 2001, ApJ, 553, 528, doi: [10.1086/320977](https://doi.org/10.1086/320977)

Fox, A. J. 2011, ApJ, 730, 58, doi: [10.1088/0004-637X/730/1/58](https://doi.org/10.1088/0004-637X/730/1/58)

Fox, A. J., Lehner, N., Tumlinson, J., et al. 2013, ApJ, 778, 187, doi: [10.1088/0004-637X/778/2/187](https://doi.org/10.1088/0004-637X/778/2/187)

Frank, S., Pieri, M. M., Mathur, S., Danforth, C. W., & Shull, J. M. 2018, MNRAS, 476, 1356, doi: [10.1093/mnras/sty294](https://doi.org/10.1093/mnras/sty294)

Fukugita, M., Hogan, C. J., & Peebles, P. J. E. 1998, ApJ, 503, 518, doi: [10.1086/306025](https://doi.org/10.1086/306025)

Gaikwad, P., Khaire, V., Choudhury, T. R., & Srianand, R. 2017, MNRAS, 466, 838, doi: [10.1093/mnras/stw3086](https://doi.org/10.1093/mnras/stw3086)

Gnat, O., & Sternberg, A. 2007, ApJS, 168, 213, doi: [10.1086/509786](https://doi.org/10.1086/509786)

Grevesse, N., Asplund, M., Sauval, A. J., & Scott, P. 2010, Ap&SS, 328, 179, doi: [10.1007/s10509-010-0288-z](https://doi.org/10.1007/s10509-010-0288-z)

Gunasekera, C. M., van Hoof, P. A. M., Dehghanian, M., et al. 2025, arXiv e-prints, arXiv:2508.01102, doi: [10.48550/arXiv.2508.01102](https://doi.org/10.48550/arXiv.2508.01102)

Hafen, Z., Faucher-Giguère, C.-A., Anglés-Alcázar, D., et al. 2017, MNRAS, 469, 2292, doi: [10.1093/mnras/stx952](https://doi.org/10.1093/mnras/stx952)

Heckman, T. M., Norman, C. A., Strickland, D. K., & Sembach, K. R. 2002, ApJ, 577, 691, doi: [10.1086/342232](https://doi.org/10.1086/342232)

Hu, T., Khaire, V., Hennawi, J. F., et al. 2023, The Impact of the WHIM on the IGM Thermal State Determined from the Low- z Lyman- α Forest. <https://arxiv.org/abs/2308.14738>

Hussain, T., Khaire, V., Srianand, R., Muzahid, S., & Pathak, A. 2017, MNRAS, 466, 3133, doi: [10.1093/mnras/stw3265](https://doi.org/10.1093/mnras/stw3265)

Hussain, T., Muzahid, S., Narayanan, A., et al. 2015, MNRAS, 446, 2444, doi: [10.1093/mnras/stu2285](https://doi.org/10.1093/mnras/stu2285)

Khaire, V., & Srianand, R. 2015, MNRAS, 451, L30, doi: [10.1093/mnrasl/slv060](https://doi.org/10.1093/mnrasl/slv060)

—. 2019, MNRAS, 484, 4174, doi: [10.1093/mnras/stz174](https://doi.org/10.1093/mnras/stz174)

Lan, T.-W., & Mo, H. 2018, ApJ, 866, 36, doi: [10.3847/1538-4357/aadc08](https://doi.org/10.3847/1538-4357/aadc08)

Lehner, N., Savage, B. D., Richter, P., et al. 2007, ApJ, 658, 680, doi: [10.1086/511749](https://doi.org/10.1086/511749)

Macquart, J.-P., Prochaska, J. X., McQuinn, M., et al. 2020, Nature, 581, 391, doi: [10.1038/s41586-020-2300-2](https://doi.org/10.1038/s41586-020-2300-2)

Martizzi, D., Vogelsberger, M., Artale, M. C., et al. 2019, MNRAS, 486, 3766, doi: [10.1093/mnras/stz1106](https://doi.org/10.1093/mnras/stz1106)

Meiring, J. D., Tripp, T. M., Werk, J. K., et al. 2013, ApJ, 767, 49, doi: [10.1088/0004-637X/767/1/49](https://doi.org/10.1088/0004-637X/767/1/49)

Mishra, S., & Muzahid, S. 2022, ApJ, 933, 229, doi: [10.3847/1538-4357/ac7155](https://doi.org/10.3847/1538-4357/ac7155)

Mishra, S., Muzahid, S., Dutta, S., Srianand, R., & Charlton, J. 2024, MNRAS, 527, 3858, doi: [10.1093/mnras/stad3454](https://doi.org/10.1093/mnras/stad3454)

Narayanan, A., Savage, B. D., Mishra, P. K., et al. 2018, MNRAS, 475, 3529, doi: [10.1093/mnras/sty042](https://doi.org/10.1093/mnras/sty042)

Narayanan, A., Savage, B. D., & Wakker, B. P. 2012, ApJ, 752, 65, doi: [10.1088/0004-637X/752/1/65](https://doi.org/10.1088/0004-637X/752/1/65)

Narayanan, A., Wakker, B. P., & Savage, B. D. 2009, ApJ, 703, 74, doi: [10.1088/0004-637X/703/1/74](https://doi.org/10.1088/0004-637X/703/1/74)

Narayanan, A., Wakker, B. P., Savage, B. D., et al. 2010, ApJ, 721, 960, doi: [10.1088/0004-637X/721/2/960](https://doi.org/10.1088/0004-637X/721/2/960)

Nicastro, F., Kaastra, J., Krongold, Y., et al. 2018, Nature, 558, 406, doi: [10.1038/s41586-018-0204-1](https://doi.org/10.1038/s41586-018-0204-1)

Oppenheimer, B. D., Davé, R., Katz, N., Kollmeier, J. A., & Weinberg, D. H. 2012, MNRAS, 420, 829, doi: [10.1111/j.1365-2966.2011.20096.x](https://doi.org/10.1111/j.1365-2966.2011.20096.x)

Pachat, S., Narayanan, A., Khaire, V., et al. 2017, MNRAS, 471, 792, doi: [10.1093/mnras/stx1435](https://doi.org/10.1093/mnras/stx1435)

Pachat, S., Narayanan, A., Muzahid, S., et al. 2016, MNRAS, 458, 733, doi: [10.1093/mnras/stw194](https://doi.org/10.1093/mnras/stw194)

Petitjean, P. 1998, arXiv e-prints, astro, doi: [10.48550/arXiv.astro-ph/9810418](https://doi.org/10.48550/arXiv.astro-ph/9810418)

Planck Collaboration, Aghanim, N., Akrami, Y., et al. 2020, A&A, 641, A6, doi: [10.1051/0004-6361/201833910](https://doi.org/10.1051/0004-6361/201833910)

Prochaska, J., Werk, J., Werk, J., et al. 2017, The Astrophysical Journal, 837, doi: [10.3847/1538-4357/aa6007](https://doi.org/10.3847/1538-4357/aa6007)

Rahmati, A., & Oppenheimer, B. D. 2018, MNRAS, 476, 4865, doi: [10.1093/mnras/sty610](https://doi.org/10.1093/mnras/sty610)

Richter, P., Savage, B. D., Sembach, K. R., & Tripp, T. M. 2006, A&A, 445, 827, doi: [10.1051/0004-6361:20053636](https://doi.org/10.1051/0004-6361:20053636)

Sameer, Lehner, N., Howk, J. C., et al. 2024, ApJ, 975, 264, doi: [10.3847/1538-4357/ad7af2](https://doi.org/10.3847/1538-4357/ad7af2)

Savage, B. D., Kim, T.-S., Wakker, B. P., et al. 2014, ApJS, 212, 8, doi: [10.1088/0067-0049/212/1/8](https://doi.org/10.1088/0067-0049/212/1/8)

Savage, B. D., & Lehner, N. 2006, ApJS, 162, 134, doi: [10.1086/497915](https://doi.org/10.1086/497915)

Savage, B. D., Lehner, N., & Narayanan, A. 2011, ApJ, 743, 180, doi: [10.1088/0004-637X/743/2/180](https://doi.org/10.1088/0004-637X/743/2/180)

Savage, B. D., Lehner, N., Wakker, B. P., Sembach, K. R., & Tripp, T. M. 2005, ApJ, 626, 776, doi: [10.1086/429985](https://doi.org/10.1086/429985)

Savage, B. D., Narayanan, A., Wakker, B. P., et al. 2010, ApJ, 719, 1526, doi: [10.1088/0004-637X/719/2/1526](https://doi.org/10.1088/0004-637X/719/2/1526)

Schaye, J., Carswell, R. F., & Kim, T.-S. 2007, MNRAS, 379, 1169, doi: [10.1111/j.1365-2966.2007.12005.x](https://doi.org/10.1111/j.1365-2966.2007.12005.x)

Shen, S., Wadsley, J., & Stinson, G. 2010, MNRAS, 407, 1581, doi: [10.1111/j.1365-2966.2010.17047.x](https://doi.org/10.1111/j.1365-2966.2010.17047.x)

Shull, J. M., Danforth, C. W., & Tilton, E. M. 2014, ApJ, 796, 49, doi: [10.1088/0004-637X/796/1/49](https://doi.org/10.1088/0004-637X/796/1/49)

Shull, J. M., Smith, B. D., & Danforth, C. W. 2012, ApJ, 759, 23, doi: [10.1088/0004-637X/759/1/23](https://doi.org/10.1088/0004-637X/759/1/23)

Simcoe, R. A., Sargent, W. L. W., & Rauch, M. 2004, ApJ, 606, 92, doi: [10.1086/382777](https://doi.org/10.1086/382777)

Smith, B. D., Hallman, E. J., Shull, J. M., & O’Shea, B. W. 2011, ApJ, 731, 6, doi: [10.1088/0004-637X/731/1/6](https://doi.org/10.1088/0004-637X/731/1/6)

Sutherland, R. S., & Dopita, M. A. 1993, ApJS, 88, 253, doi: [10.1086/191823](https://doi.org/10.1086/191823)

Tejos, N., Prochaska, J. X., Crighton, N. H. M., et al. 2016, MNRAS, 455, 2662, doi: [10.1093/mnras/stv2376](https://doi.org/10.1093/mnras/stv2376)

Tepper-García, T., Richter, P., Schaye, J., et al. 2012, MNRAS, 425, 1640, doi: [10.1111/j.1365-2966.2012.21545.x](https://doi.org/10.1111/j.1365-2966.2012.21545.x)

Thom, C., & Chen, H.-W. 2008a, ApJS, 179, 37, doi: [10.1086/591232](https://doi.org/10.1086/591232)

—. 2008b, ApJ, 683, 22, doi: [10.1086/587976](https://doi.org/10.1086/587976)

Tripp, T. M., & Savage, B. D. 2000, ApJ, 542, 42, doi: [10.1086/309506](https://doi.org/10.1086/309506)

Tripp, T. M., Sembach, K. R., Bowen, D. V., et al. 2008, ApJS, 177, 39, doi: [10.1086/587486](https://doi.org/10.1086/587486)

Tumlinson, J., Peebles, M. S., & Werk, J. K. 2017, ARA&A, 55, 389, doi: [10.1146/annurev-astro-091916-055240](https://doi.org/10.1146/annurev-astro-091916-055240)

Tumlinson, J., Thom, C., Werk, J. K., et al. 2013, ApJ, 777, 59, doi: [10.1088/0004-637X/777/1/59](https://doi.org/10.1088/0004-637X/777/1/59)

Tuominen, T., Nevalainen, J., Tempel, E., et al. 2021, A&A, 646, A156, doi: [10.1051/0004-6361/202039221](https://doi.org/10.1051/0004-6361/202039221)

Werk, J. K., Prochaska, J. X., Cantalupo, S., et al. 2016, ApJ, 833, 54, doi: [10.3847/1538-4357/833/1/54](https://doi.org/10.3847/1538-4357/833/1/54)

Williger, G. M., Heap, S. R., Weymann, R. J., et al. 2006, ApJ, 636, 631, doi: [10.1086/498127](https://doi.org/10.1086/498127)

Yang, L., Zheng, Z., du Mas des Bourboux, H., et al. 2022, ApJ, 935, 121, doi: [10.3847/1538-4357/ac7b2e](https://doi.org/10.3847/1538-4357/ac7b2e)